

# Correlation of measurements $\text{OH}^*$ , $\text{CH}^*$ , $\text{C}_2^*$ and $\text{H}_2\text{O}$ with changing signal of Electrical Capacitance Tomography system in the reaction zone of methane/air premixed flames

Zbigniew Gut \*

## Abstract

Research into the application of Electrical Capacitance Tomography (ECT) carried out in the Laboratory of the Aircraft Engines Division at Warsaw University of Technology has shown that it is applicable to recognition of various flames. Several cases were tested using the ECT system and the system successfully created cross sectional images of premixed and diffusion flames. Studies were then conducted which significantly increased the functionality of the system.

This article describes experimental studies that afforded insight into the effects of the degree of ionization generated during the combustion process on the changing signal of the ECT system. Research was carried out in an experimental stand consisting of a burner, 6 and 12 electrodes capacitance sensors and an optical spectrometer. Burner injection was used to obtain stability of combustion. Two rotameters were installed in the inlet of the burner. The flow rate of air and methane was used to determine the composition of the combustible mixture formed in the mixing chamber. A grating spectrometer was used to perform a detailed analysis of combustion processes and to detect various types radicals. This experimental test focused on measuring chemiluminescence intensities and possible correlations of the  $\text{OH}^*$ ,  $\text{CH}^*$ ,  $\text{C}_2^*$  and  $\text{H}_2\text{O}$  with air/methane ratio. The data from the ECT system and optical spectrometer was then analyzed. It was found that the strong correlations between the peak intensity of  $\text{OH}^*$ ,  $\text{CH}^*$ ,  $\text{C}_2^*$  and  $\text{H}_2\text{O}$  in the reaction zone to the equivalence ratio could be used to investigate the local flame stoichiometry.

**Keywords:** combustion process, visualization, tomography, spectrometer

## 1 Introduction

The development of diagnostic methods for the monitoring of flames in practical applications is an important objective and one which is receiving growing attention and attracting significant research efforts. This is motivated by the need to achieve more detailed

knowledge of the process and to implement efficient and reliable control and optimization methods as a key step towards developing more efficient, flexible, reliable and clean combustion systems. Many advanced and interesting solutions have been proposed, involving a wide range of different approaches in terms of the instrumentation utilized and concepts proposed to convert sensorial information into various meaningful parameters.

Traditionally, combustion processes have been monitored by optical means, using techniques such as Schlieren [1], shadow, interferometric [2], holographic and planer laser-induced fluorescence [3]. But in these methods, high quality optical access to the area of interest is required. However, utilization of the above in industrial conditions is difficult.

One of the harder to control parameters is distribution of the reaction zone. Presently, there is no system in existence that delivers continuous monitoring of combustion processes in industrial burners or aircraft engines. Measurements of temperature or control of existing flame by using an ionization probe [4]; [5] provide only partial information about performance of the combustion process. For that reason, new diagnostic methods should be developed. While many interesting attempts have been proposed to date, one of the most interesting solutions is the development of combustion process diagnostic methods by means of Electrical Capacitance Tomography (ECT).

Currently, the main aim of Capacitance Tomography is to obtain images of permittivity distribution in gas flow systems, a dense pneumatic conveying system or bubbling fluidization [6]; [7]; [8]; [9]; [10].

The basic idea of ECT is to measure changes in electrical capacitances between all possible combinations of electrodes when a dielectric material is introduced into the measurement space. These inter-electrode capacitance changes are caused by variations in the distribution permittivity of the material inside the vessel. An ECT system has three main units: the sensor, sensing electronics and computer, as are shown in Fig-

\*Institute of Aviation Center of Space Technologies Space Technologies Division al. Krakowska 110/114 02-256 Warsaw, POLAND, e-mail

Figure 1.

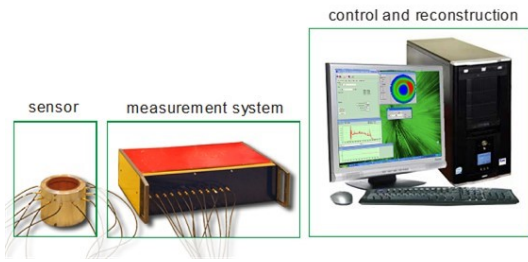


Figure 1: Elements of the Electrical Capacitance Tomography system

The sensor consists of a set of electrodes symmetrically mounted outside or inside a chamber. The sensing electronics measure the capacitances for all possible electrode combinations. The computer system has two major functions. Firstly, it controls the measurement operations performed by the sensing electronics; secondly, it uses the measurement data to reconstruct tomographic images as well as presents and interprets them.

Previous studies were based on reconstruction of the reaction zone structure of non-premixed and premixed flames. In the research, the flame structure and its location in the combustion chamber were observed and registered [11]; [12]; [13]. The next step was to conduct studies which significantly increased the functionality of the system. This includes the ability to use the ECT system to control the composition of the mixture. Some examples are shown in Figure 2.

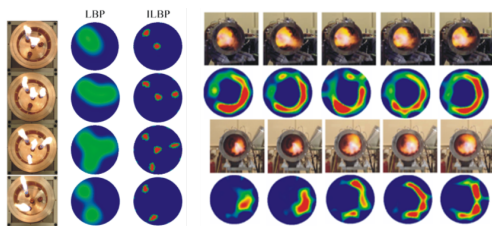


Figure 2: Reconstruction of diffusion flame and combustion process inside the chamber of GTD-350 engine [11].

As opposed to classical applications of the ECT system, in the reconstruction of the combustion process the signal level depends on the concentrations of various kinds of charged particles present during the combustions. These charged particles may be formed as a result of chemical reactions, called chemi-ionization and thermal ionization. They are modified by the permittivity and conductivity of the reaction zone [14].

Lawton proved that the flame in the variable electric field behaves like a dielectric and conductor. Classical electrodynamics give expressions for the dielectric constant and conductivity of a medium containing free ionic species, so this parameter varies with the angular and collision frequency and flame characteristics.

To understand the processes taking place in the flame, it is important to gain knowledge about the concentrations of the various kinds of species. Optical spectrometry is helpful to that end. Optical emissions from flames are widely used in combustion sensing and diagnostic applications. The energy emitted by a flame is spectrally distributed in the ultraviolet (UV), visible (VIS) and infrared (IR) regions, and it has been classified in continuous and discontinuous spectra. Continuous spectra are generally observed in the sooty region of hydrocarbon flames, where energy is distributed in a wide band of wavelengths. Usually a maximum intensity is achieved within such band. The discontinuous spectra are attributed to the emitted energy by isolated atoms or molecules, where the energy is mainly confined around a certain narrow band region of wavelengths, arranged in groups called free radical bands.

The formation mechanisms of excited radicals are not yet completely understood, but some key reactions have been identified. The formation process of  $\text{OH}^*$  and  $\text{CO}_2^*$  is well documented. Reactions leading to  $\text{CH}^*$  have also been investigated, but more work is still needed for  $\text{C}_2^*$  [15]; [16]; [17]; [18].

One interesting feature of chemiluminescence used for combustion control is that it may be related to several important flame parameters. In many publications, correlations between chemiluminescence and equivalence ratio have been reported [19]; [20].

## 2 Design and construction of a gas burner with a mixer

A burner is a device that supplies the combustion process substrates and thereby determines its performance and provides near its outlet spatial stability of combustion. The simplest design of burner used in the diagnosis of combustion is an injection type burner. A gas burner of this type consists of a gas nozzle, air nozzle, mixing chamber and flame stabilizer. The mixing chamber was used to produce a homogeneous mixture of gas and air. In order to reduce the dimensions of the chamber and to increase the intensity of mixing, an intersection stream of gas and air was used. The stabilizer is meant to prevent the flame jumping to the inside of the mixer and to preclude the flame detaching from the burner. These guidelines aid the design and manufacture of the burner elements. The

diameter of the outlet burner was 10 mm and the height was 100 mm. Figure 3 shows the individual components of the burner.

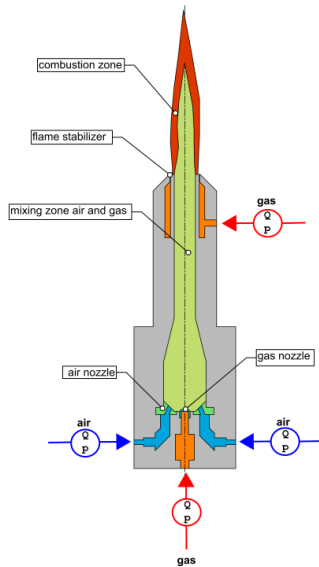


Figure 3: Schematic diagram of a gas burner

The stoichiometry ratio of mixture was determined by using the formula:

$$\lambda = \frac{\left(\frac{A}{F}\right)_e}{\left(\frac{A}{F}\right)_s} = \frac{\left(\frac{m_{air}}{m_{CH_4}}\right)_e}{\left(\frac{A}{F}\right)_s}$$

where:  $(A/F)_e$  – experimental air-to-fuel ratio;  $(A/F)_s$  – stoichiometric air-to-fuel ratio for methane  $(A/F)_s=9.52$ .

Individual components of the experimental stand are shown in Figures 4 and 5.



Figure 4: View of experimental stand

The construction was designed so that some parts are replaceable. For example, the appropriate shaping of the holes in the air nozzle delivers optimal conditions for preparation of the combustible mixture. Additionally, thanks to the replaceable elements, it was possible to adapt the process of preparing the mixture, depending on the research needs.

### 3 Experimental stand

The measuring stand consists of two independent power supply systems: air and gaseous fuel. Flammable gas is supplied from the cylinder through a pressure reducer. Behind the pressure reducer, a gas fuse has been installed, which effectively protects the gas and gas network against backflow and flame retardation. The gas stream was divided into two points. A small stream of flammable gas was supplied to the burner, into the flame stabilization zone. In this way, a small pilot flame was created in the vicinity of the air outlet, facilitating a stable combustion process over a wide range of compositions (Fig. 6). Air was supplied from the compressed air system and a buffer tank, where a pressure reducer was also used.

The most important elements of each feed were the air and fuel gas flow metering systems. In this case, two independent rotameters were used. Control of mass air flow  $m_{air}$  and mass fuel gas flow  $m_{CH_4}$  were achieved through the use of needle valves.

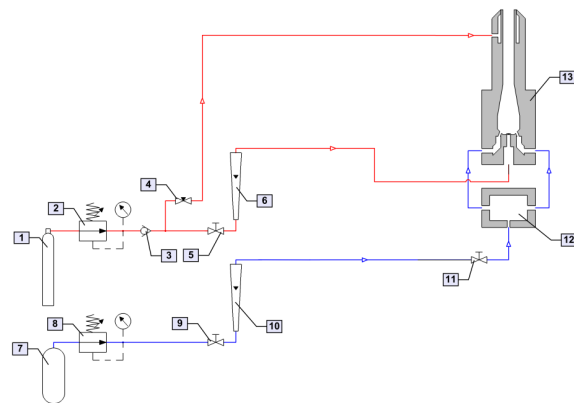


Figure 5: Schematic diagram of experimental stand (1 - gas cylinder; 2 - pressure reducer; 3 - safety valve; 4 - valve; 5 - needle control valve for fuel delivery to the burner; 6- rotameter; 7- air tank; 8 - pressure reducer; 9 - needle regulating valve for supplying air to the burner; 10 - rotameter; 11 - valve; 12 - buffer air tank; 13 - burner)

The conditioning of flame stabilization in a flow field was carried out. The tests of flame stability of the burner consisted of: in the first place a constant flow of gaseous fuel was set, and then the air flow rate was increased until the flame was extinguished. The test procedure for a burner with and without a flame stabilizer was performed and the results are shown in Figure 7.

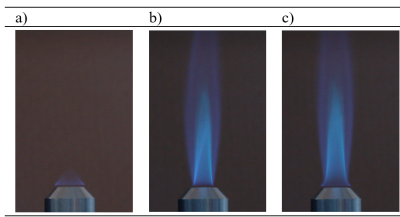


Figure 6: Pictures of flame ( $m_{\text{CH}_4}=0.1 \text{ m}^3/\text{kg}$ ,  $m_{\text{Air}}=0.7 \text{ m}^3/\text{kg}$ ) a) stabilizing flame, b) flame without stabilization, c) flame with stabilization

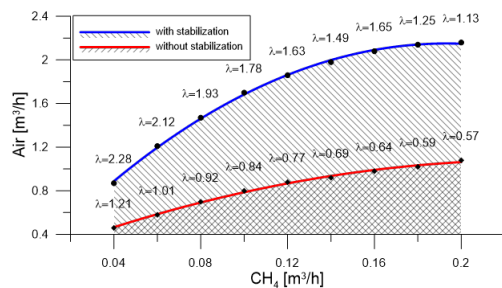


Figure 7: Diagram of changes in the composition of mixtures with and without stabilizer

The research conducted shows that the use of a pilot flame enables the range of mixtures to be increased significantly. By using the stabilizer we can carry out measurements across a wide range of mixtures, from rich to lean. This applies mainly to poor mixtures where too high a velocity of mixture outflow adversely impacts the stability of combustion.

## 4 Design and performance of the electrodes

The sensor is a key element of Electrical Capacitance Tomography. ECT is a non-invasive measuring method, so the principle of construction of the sensor is based on placing a set of electrodes around the measurement area, so that the flow or distribution medium inside the tank is not disturbed. Its construction is adapted to the environment in which it comes to work as well as the geometry of the component test. If the vessel wall is non-conducting, capacitance electrodes can be located inside, within or outside the wall. However, if the tube wall is a conductor, internal electrodes must be used. A typical sensor consists of four main parts: measurement electrodes, an insulating frame, outer, axial end and radial screens and coaxial cables and connectors. In our case, where we deal with relatively high temperatures, electrodes are placed inside the chamber. In this construction, because of the small size of the sensor, we must aban-

don the axial and radial screens, and the only earthed screen is a pipe.

Previous research [21]; [22] has shown that the optimal number of electrodes, from the point of radial resolution, is twelve, but for comparison 6 sensor electrodes were also used. The diameter of the sensor was chosen so that its value, 34 mm, was approximately 10% greater than the diameter of the flame. Due to the fact that the flame has conductive properties, contact with the electrodes may cause significant disturbances in the reconstructed image.

Each electrode was isolated from the chamber wall with insulating material (ceramic). Additionally, by using the SMB connectors, we were able to connect each electrode to the measurement device. To obtain a suitable signal-to-noise ratio and high axial resolution, the lengths of the electrodes were determined by numerical methods. The length for the 12 electrode system was 25 mm and for the 6 electrode sensor it was 13 mm. In Electrical Capacitance Tomography we always must find a compromise between: the number of electrodes, electrode size, resolution and sensitivity of the system. The design of the sensor and its individual elements are presented in Figure 8.

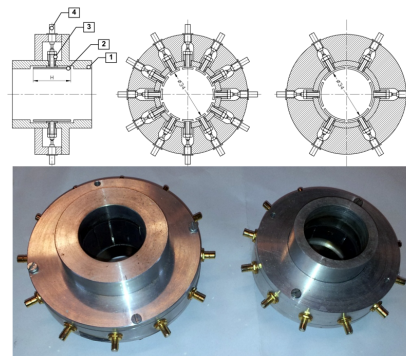
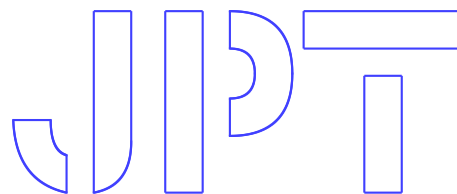


Figure 8: A cross section and view of the 6 and 12 electrode sensors (1 – body of sensor, 2 - electrode, 3 - ceramic insulation, 4 - connector)

## 5 Spectrometer

A spectrometer is a simple optical instrument based on a diffraction grating and a one-dimensional CCD detector array. A Silver-Nova spectrometer was used in this investigation, as shown in Figure 9. The Silver-Nova is a good all-purpose spectrometer, giving research grade results for numerous spectroscopic applications over the 190-1110 nm wavelength range and a spectral resolution of about 0.5 nm with a 25 um slit. The CCD array of the spectrometer has  $1 \times 2048$  pixels so the spectrum reads out as a list of 2048



data numbers. The spectrograph employs composite grating technology to deliver high efficiency in both the UV & NIR spectral extremes. The UV enhanced CCD detector with integrated TE cooler, gain enhancements, and optical lens assemblies allow for unparalleled sensitivity, with over 65% increased signal to noise at long exposures. Additionally, the metal enclosure is ruggedized and compact to allow for portable, process, or laboratory environments.



Figure 9: Silver-Nova super range TEC spectrometer

The system can configure all instrument parameters, plotting spectral data in “Scope mode”, “Absorbance mode”, “Transmission mode”, and even “Irradiance mode”. The maximum light intensity is 65536 (16-bit) in this model of spectrometer. “Scope mode” was used during our research. “Scope Mode” simplifies the charts of spectral power distribution in units of counts (y-axis) versus wavelength  $\Lambda$  (x-axis). It is important to understand that the spectrum displayed in “Scope Mode” does not let you infer quantitative or qualitative information about a light source. In other words, the measurements only enable you to determine the nature of changes of individual radicals.

When configuring a spectrometer for an experiment, one commonly overlooked consideration is the choice of suitable fiber optic cable. This enables light to be easily transferred from a light source to a spectrometer for spectra detection. For StellarNet systems the 600 $\mu$ m fiber diameter is the most popular and provides a high light signal. In our case, fiber optic cable F600-UVVis-SR was used. Typically, optical fibers are not resistant to high temperatures and therefore it was necessary to locate them at a distance from the flame. In our case, the distance was 65 mm.

A very important task in spectrometric studies was to determine the individual radicals taken from the emission spectrum of a flame. For this purpose the book “The spectroscopy of flames” by A.G. Gaydon was used. In Figure 10 and Table 1 the identified radicals are shown.

We can see that high-temperature gaseous flames emit both visible and ultraviolet light as a result of energy level transitions of the electrons in the molecules. Such transitions are observed as band spectra, which are due to changes in the vibrational and rotational

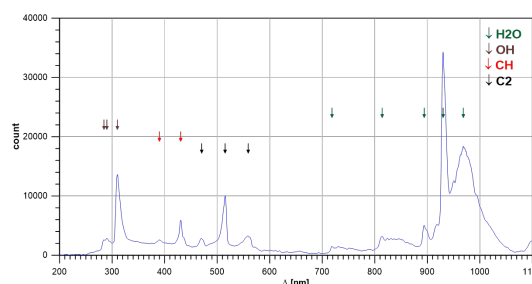


Figure 10: Typical recorded sample spectra for stoichiometric methane-air mixture

Table 1: Identified radicals

Radicals	$\Lambda$ nm
OH*	284.5, 290, 310
CH*	390, 430.5
C <sub>2</sub> *	470.5, 515, 559
H <sub>2</sub> O	718.5, 814, 894, 930, 968.5

energies of the molecules. In our case, in this spectral range, we can observe that the methane/air flame produces H<sub>2</sub>O molecules and three types of radical: OH\*, CH\* and C<sub>2</sub>\*.

## 6 Research - optical spectrometer

In the first stage of research, for different mixture composition, for the methane-air flame the emission spectrum of individual radicals was determined. Two variants of the research were assumed. The first variant consisted of providing a constant flow rate of flammable gas with variable flow rate of air. The second option consisted of providing a constant air flow rate with variable flow rate of flammable gas. For each variant, three values flow rate of air ( $m_{air}=0.8, 1.0, 1.2$  m<sup>3</sup>/h) and gas ( $m_{CH_4}=0.10, 0.12, 0.14$  m<sup>3</sup>/h) were selected. On the basis of recorded measurement data of the flow rate and pressure of combustible gas and air, the composition of the combustible mixture was determined, where the stoichiometric coefficient ranged from 0.6 to 1.4 in atmospheric pressure.

The signal changes at various heights from the burner outlet: 15, 25, 35, 45, 50, 55, 65 mm were recorded as shown in Figure 11.

The data obtained from the optical spectrometer to a value of 0 and 1 were normalized with the formula:

$$Norm = \frac{\text{light intensity}}{65536}$$

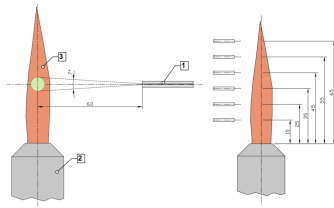


Figure 11: Schematic of measurement points (1 - fiber optic cable; 2 - burner; 3 – flame)

For individual radicals of OH\* for the spectrum 310 nm, CH\* for spectrum 430.5 nm, C<sub>2</sub>\* for spectrum 515 nm, H<sub>2</sub>O for spectrum 930 nm, sum of ΣOH\* and ΣC<sub>2</sub>\* radicals, sum of ΣH<sub>2</sub>O molecules and the sum of all radicals and molecules Σ\* as a function of the mixture were plotted.

Analysis of the data obtained is shown in Figure 12 where the maximum concentration of the sum of all radicals and molecules occurs at a height of 35 mm from the burner outlet. For this purpose, the article focuses only on presenting the results at this level.

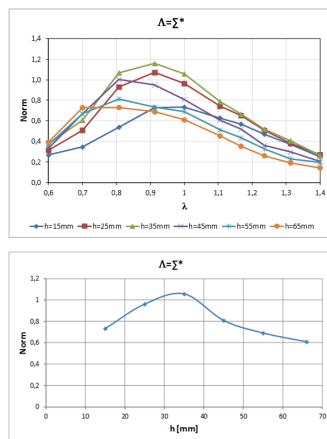


Figure 12: Relationship between the composition mixture and the signals of sum molecules and radicals and profiles of changes in intensity as a function of position of the fiber optic cable

Intensity profiles in methane-air flame of OH\*, CH\*, C<sub>2</sub>\*, H<sub>2</sub>O, ΣOH\*, ΣC<sub>2</sub>\*, ΣH<sub>2</sub>O and Σ\* as a function of composition mixture for different constant mass flow rates of air and methane were made and shown in Figures 13, 14, 15 and 16.

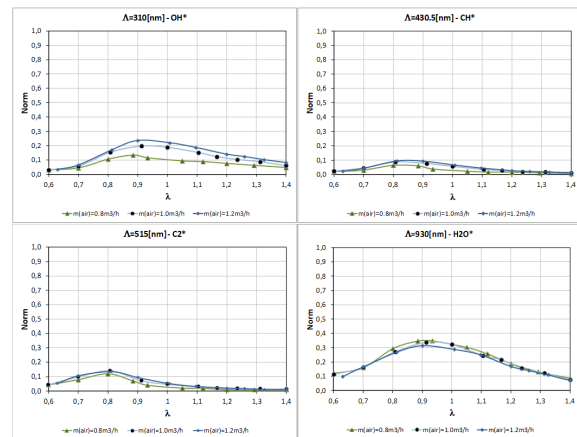


Figure 13: Intensity profiles in methane-air flame of OH\*, CH\*, C<sub>2</sub>\* and H<sub>2</sub>O as a function of composition mixture for different constant mass flow rates of air, m<sub>air</sub>=0.8, 1.0, 1.2 m<sup>3</sup>/h

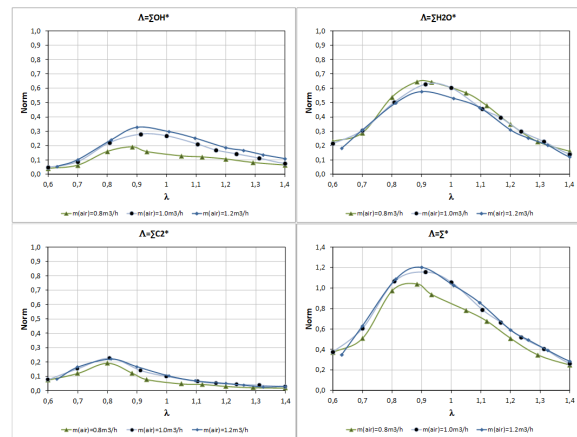


Figure 14: Intensity profiles in methane-air flame of ΣOH\*, ΣC<sub>2</sub>\*, ΣH<sub>2</sub>O and Σ\* as a function of composition mixture for different constant mass flow rates of air, m<sub>air</sub>=0.8, 1.0, 1.2 m<sup>3</sup>/h

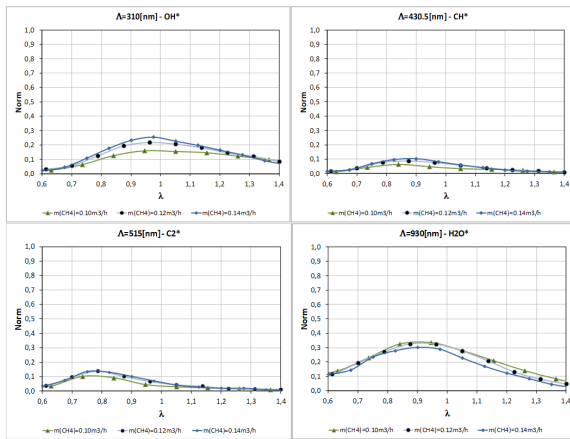


Figure 15: Intensity profiles in methane-air flame of  $\text{OH}^*$ ,  $\text{CH}^*$ ,  $\text{C}_2^*$  and  $\text{H}_2\text{O}$  as a function of composition mixture for different constant mass flow rates of  $\text{CH}_4$ ,  $m_{\text{CH}_4}=0.10, 0.12, 0.14 \text{ m}^3/\text{h}$

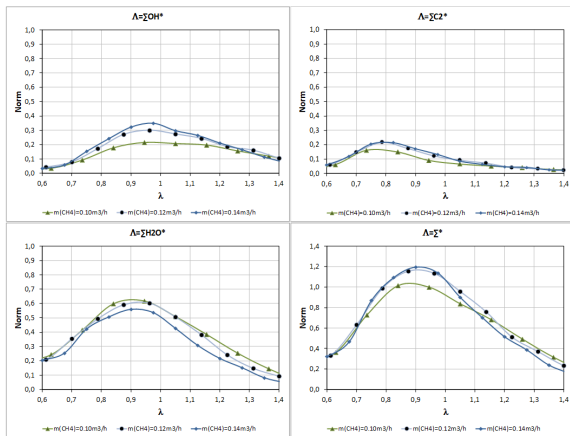


Figure 16: Intensity profiles in methane-air flame of  $\Sigma\text{OH}^*$ ,  $\Sigma\text{C}_2^*$ ,  $\Sigma\text{H}_2\text{O}$  and  $\Sigma^*$  as a function of composition mixture for different constant mass flow rates of  $\text{CH}_4$ ,  $m_{\text{CH}_4}=0.10, 0.12, 0.14 \text{ m}^3/\text{h}$

## 7 Research - Electrical Capacitance Tomography

The research with the use of ECT system consisted of the recording of changes in signal from individual electrode pairs for different compositions of mixtures. Usually, the capacitance measurements obtained from the ECT system are normalized at high and low permittivity for image reconstruction. The normalized capacitance is “0” when the sensor is full of low permittivity material, and “1” when it is full of high permittivity material. In our experiment, a sensor was calibrated using air as lower permittivity material and plastic rod ( $\epsilon \sim 2.4$ ) as higher permittivity material.

Methane was used as fuel and two identical variants of the test were assumed, which were used in studies using an optical spectrometer. For each variant, the signal changes were measured for the 6 and 12 electrode sensors as well as for two height positions of the sensor center from the burner outlet: 35 mm and 55 mm. A schematic diagram of the location of the sensor used in research is shown in Figure 17. The first sensor height of 35 mm was dictated by the results obtained using an optical spectrometer, where the intensity of sum molecules and radicals was highest. For control purposes, additional measurements were performed at a second height.

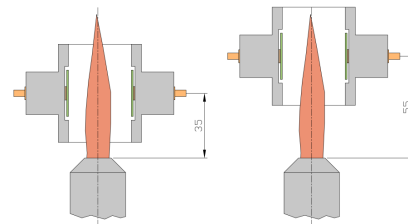


Figure 17: Schematic diagram of the location of the sensor used in research

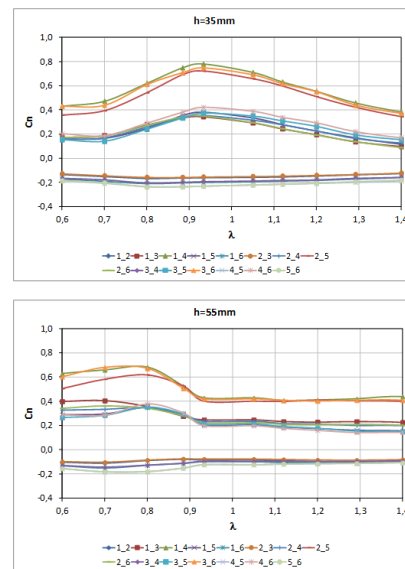


Figure 18: Profile of signal change as a function of composition mixture for the 6 electrode sensor and constant air  $m_{\text{air}}=0.8 \text{ m}^3/\text{h}$

The analysis of the measurement data in Figure 18 showed that the measurements at 55 mm do not have such characteristic changes in signal as a function of the composition mixture as they do for the height of 35 mm. For this reason, in the further analysis, only the data that was recorded at the height of 35 mm will be given. Also, as can

be seen, signals from the pairs of neighboring electrodes ( $C_{1-2}, C_{1-6}, C_{2-3}, C_{3-4}, C_{4-5}, C_{5-6}$ ) are rather unhelpful. First of all, the changes are unnoticeable and take negative values.

Several formulas were used for data analysis:

- for the 6 electrode sensor:
  - o mean - average value from all pairs of electrodes;
  - o  $\text{mean}(C_{1-4}, C_{2-5}, C_{3-6})$  - average value from the opposing electrode pairs;
  - o  $\text{mean}(C_{1-3}, C_{1-5}, C_{2-4}, C_{2-6}, C_{3-5}, C_{4-6})$  - mean value from electrode pairs separated by one electrode;
- for the 12 electrode sensor:
  - o mean - average value from all pairs of electrodes;
  - o  $\text{mean}(C_{1-7}, C_{2-8}, C_{3-9}, C_{4-10}, C_{5-11}, C_{6-12})$  - average value from the opposing electrode pairs.

The graphs of signal changes as a function of the composition of the mixture for individual variants were made and shown in Figures 19, 20, 21, 22.

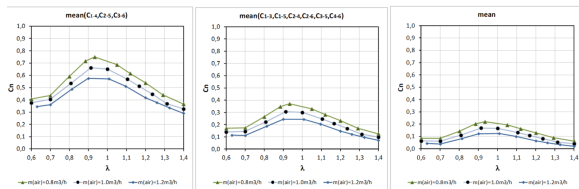


Figure 19: Profile of signal change as a function of composition mixture for the 6 electrode sensor and at constant air flow rates  $m_{\text{air}}=0.8, 1.0, 1.2 \text{ m}^3/\text{h}$

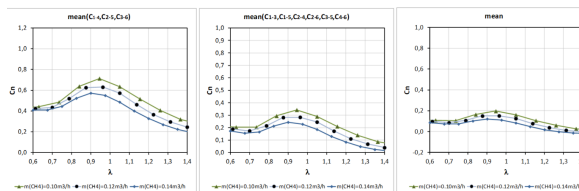


Figure 20: Profile of signal change as a function of composition mixture for the 6 electrode sensor and at constant  $\text{CH}_4$  flow rates  $m_{\text{CH}_4}=0.10, 0.12, 0.14 \text{ m}^3/\text{h}$

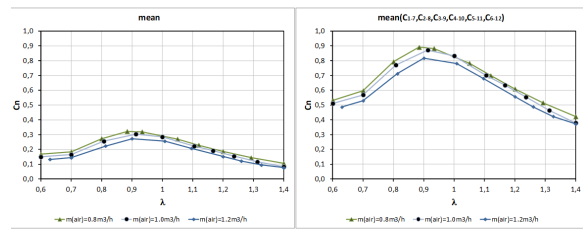


Figure 21: Profile of signal change as a function of composition mixture for the 12 electrode sensor and at constant air flow rates  $m_{\text{air}}=0.8, 1.0, 1.2 \text{ m}^3/\text{h}$

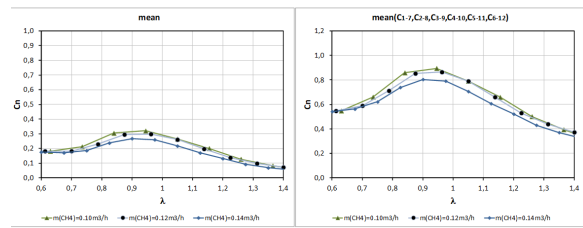


Figure 22: Profile of signal change as a function of composition mixture for the 12 electrode sensor and at constant  $\text{CH}_4$  flow rates  $m_{\text{CH}_4}=0.10, 0.12, 0.14 \text{ m}^3/\text{h}$

## 8 Conclusions

Most research centers have focused on the use of ECT to monitor two-phase flows, whereas our main purpose has been to use the capacitance tomography system to monitor combustion processes. Previous research has focused on reconstruction of the location and structure of the flame or combustion process. However, recent studies have shown that the ECT system can be used to monitor the composition of combustible mixtures too. The research we conducted proved that the level of signal changes depends on the degree of ionization. It was found that the strong correlations between the peak intensity of  $\text{OH}^*$ ,  $\text{CH}^*$ ,  $\text{C}_2^*$  and  $\text{H}_2\text{O}$  in the reaction zone to the equivalence ratio could be used to investigate local flame stoichiometry. The test results also showed that proper placement of the sensor is an important aspect of the system. This way we were able to get good correlation with signal level as a function of composition mixture.

The main disadvantage of this technique is its lower spatial resolution compared to other tomographic imaging techniques and optical systems. Despite this drawback it is a very good tool that can be used in research and diagnostics of many combustion systems. It is especially useful for monitoring the combustion process and has a major advantage over optical visualization systems since it does not require optical

access and uses passive, non-invasive electrodes. By continuously monitoring combustion, it will not only be possible to increase safety, but the tool may also be used to control combustion processes and improve the efficiency of heating systems. It may also prove useful for research and in the development of new combustion chambers operating at very high pressure, where the installation of optical windows is problematic or even impossible.

### Acknowledgements

The authors would like to thank the National Science Center of Poland for supporting this work in the framework of UMO-2013/09/B/ST8/01735.

### References

1. Taylor, H.G., and Waldram, J.M. (1933) Improvements in the schlieren method. *Journal of Scientific Instruments*, **10**.
2. R. South, B.M.H. (1976) Temperature Measurement in Conical Flames by Laser Interferometry. *Combustion Science and Technology*, **12**.
3. Seitzman, J.M., Kychakoff, G., and Hanson, R.K. (1985) Instantaneous temperature field measurements using planar laser-induced fluorescence. *Opt Lett*, **10**, 439–41.
4. Blizard, N., and Keck, J. (1974) Experimental and Theoretical Investigation of Turbulent Burning Model for Internal Combustion Engines. *SAE Technical Paper 740191*.
5. Yoshiyama, S., and Tomita, E. (2002) Combustion Diagnostics of a Spark Ignition Engine Using a Spark Plug as an Ion Probe. *SAE Technical Paper Series*.
6. (1989) Tomographic imaging of two-component flow using capacitance sensors. *Journal of Physics E: Scientific Instruments*, **22**.
7. (2001) Electrical capacitance tomography measurements on the pneumatic conveying of solids. *Industrial & Engineering Chemistry Research*, **40**.
8. A.J. Jaworski, T.D. (2001) Measurement Science and Technology Application of electrical capacitance tomography for measurement of gas-solids flow characteristics in a pneumatic conveying system. *Measurement Science and Technology*, **12**.
9. (2006) Application of electrical capacitance tomography for bulk solids flow analysis in silos. *Particle and Particle Systems Characterization*, **23**.
10. Liu, S., Wang, H., Jiang, F., and Yang, W.Q. (2002) A new image reconstruction method for tomographic investigation of fluidized beds. *AIChE Journal*, **48** (8), 1631–1638.
11. Z. Gut (2016) Selected application of electrical capacitance tomography in monitoring of combustion process. *Transactions of the Institute of Aviation*, **4**.
12. Waterfall, R.C. (2000) Imaging combustion using electrical capacitance tomography. *IEE Seminar on Advanced Sensors and Instrumentation Systems for Combustion Processes*.
13. CHEN, Q., and LIU, S. (2012) Flame Imaging in Meso-scale Porous Media Burner Using Electrical Capacitance Tomography. *Chinese Journal of Chemical Engineering*, **20** (2), 329–336.
14. Lawton J., W.F.J. (1969) *Electrical Aspects of Combustion*, Clarendon Press, Oxford, UK.
15. Kojima, J., Ikeda, Y., and Nakajima, T. (2005) Basic aspects of OH(A) CH(A), and C2(d) chemiluminescence in the reaction zone of laminar methane-air premixed flames. *Combustion and Flame*, **140** (1-2), 34–45.
16. PANOUTSOS, C., HARDALUPAS, Y., and TAYLOR, A. (2009) Numerical evaluation of equivalence ratio measurement using OH\* and CH\* chemiluminescence in premixed and non-premixed methane-air flames. *Combustion and Flame*, **156** (2), 273–291.
17. Ikeda, Y., Kojima, J., Nakajima, T., Akamatsu, F., and Katsuki, M. (2000) Measurement of the local flamefront structure of turbulent premixed flames by local chemiluminescence. *Proceedings of the Combustion Institute*, **28** (1), 343–350.
18. Bowman, C.T., and Seery, D.J. (1968) Chemiluminescence in the high-temperature oxidation of methane. *Combustion and Flame*, **12** (6), 611–614.
19. Docquier, N., and Candel, S. (2002) Combustion control and sensors: a review. *Progress in Energy and Combustion Science*, **28** (2), 107–150.
20. DANDY, D.A.V.I.D.S., and VOSEN, S.T.E.V.E.N.R. (1992) Numerical and Experimental Studies of Hydroxyl Radical Chemiluminescence in Methane-Air Flames. *Combustion Science and Technology*, **82** (1-6), 131–150.
21. Yang, Y., and Peng, L. (2013) A configurable electrical capacitance tomography system using a combining electrode strategy. *Measurement Science and Technology*, **24** (7), 074005.
22. Ye, J., Wang, H., and Yang, W. (2016) Evaluation of electrical capacitance tomography sensor based on the coupling of fluid field and electrostatic field. *Measurement Science and Technology*, **27** (7), 074003.